ADVANCED FUNCTIONAL MATERIALS
www.afm-journal.de

Non-Chemical Route to PGM-Free via N^+ Ion Implantation in Vertically Aligned Carbon Nanotubes

Valerio C.A. Ficca, Marco Sbroscia, Elena Stellino, Ilaria Rago, Francesco Goto, Isheta Majumdar, Gianluca Cavoto, Francesco Pandolfi, Alberto Calloni, Andrea Lucotti, Gianlorenzo Bussetti, and Ernesto Placidi**

The continuous research on electrocatalytic nanomaterials for critical raw materials replacement has returned the important class of Platinum-group-metal-free electrocatalysts (PGM-free), based on C, N, and non-noble transition metals. PGM-free are employed in Fuel Cells, Zinc-Air batteries, and Electrolyzers to catalyze important energy-related reactions. They are usually synthesized following a chemical route based on mixing, pyrolyzing, and postprocessing of specific N- and transition metal-containing compounds into conductive C structures, leading to a high content of byproducts. Herein, for the first time, a new approach for PGM-free synthesis is investigated, based on nitrogen implantation via ion beam produced with a Kaufman apparatus, and iron evaporation inside a clean chamber. The performed investigation, based on a model sp^2 carbonaceous material (vertically aligned carbon nanotubes), showed similarities to the chemical route in terms of surface functionalization with the possibility to maximize the pyridinic N content, paving the way for the first time to the synthesis of nitrogen-compound-free nanoelectrocatalysts.

1. Introduction

The development of efficient and cost-effective catalysts is essential for advancing renewable energy technologies and addressing environmental challenges. Among them, platinum group metals (PGMs), including platinum, palladium, and ruthenium have traditionally been utilized as catalysts in various electrochemical applications, such as fuel cells, due to their high catalytic activity and stability. However, the scarcity, high cost, and environmental concerns associated with PGMs have motivated extensive research into alternative catalyst materials that are abundant, cost-effective, and environmentally benign.[1–4]

The most promising alternative relies on PGM-free electrocatalysts, atomically dispersed metal-containing nanostructured materials able to catalyze reactions in energy conversion-related devices such as Fuel Cells (FC), Zinc-Air Batteries (ZAB), and Electrolyzers (EC).[5–10] In addition, their peculiar composition and structure are also useful for other reactions meant to mitigate and annul the anthropogenic impact on the environment, such as CO_2 reduction, N_2 reduction, ammonia oxidation, and nitrite detection.[7,9,11–13]

The main elements composing PGM-free are carbon, nitrogen, and first-row transition metals, usually Fe, Co, or Mn, intended to replace expensive and less abundant noble metals. The structural units of the nanomaterial can be considered graphene-like sp^2 C domains alloyed with N creating defects in the planar structure that can accommodate a single ion of the metal through coordination bonding. In PGM-free, the presence of graphitic

V. C. Ficca, M. Sbroscia, G. Cavoto, E. Placidi
Department of Physics
Sapienza University of Rome
Piazzale Aldo Moro 2, Rome 00185, Italy
E-mail: valerio.ficca@uniroma1.it; ernesto.placidi@uniroma1.it
V. C. Ficca
Department of Chemistry
Sapienza University of Rome
Piazzale Aldo Moro 5, Rome 00185, Italy

The ORCID identification number(s) for the author(s) of this article can be found under https://doi.org/10.1002/adfm.202413308

DOI: 10.1002/adfm.202413308

E. Stellino
Department of Basic and Applied Science for Engineering
Sapienza University of Rome
Piazzale Aldo Moro 2, Rome 00185, Italy
I. Rago, G. Cavoto, F. Pandolfi
INFN Rome
Piazzale Aldo Moro 2, Rome 00185, Italy
F. Goto, I. Majumdar, A. Calloni, G. Bussetti
Department of Physics
Politecnico di Milano
piazza Leonardo da Vinci 32, Milan 20133, Italy
A. Lucotti
Department of Chemistry, Materials and Chemical Engineering
Politecnico di Milano
piazza Leonardo da Vinci 32, Milan 20133, Italy

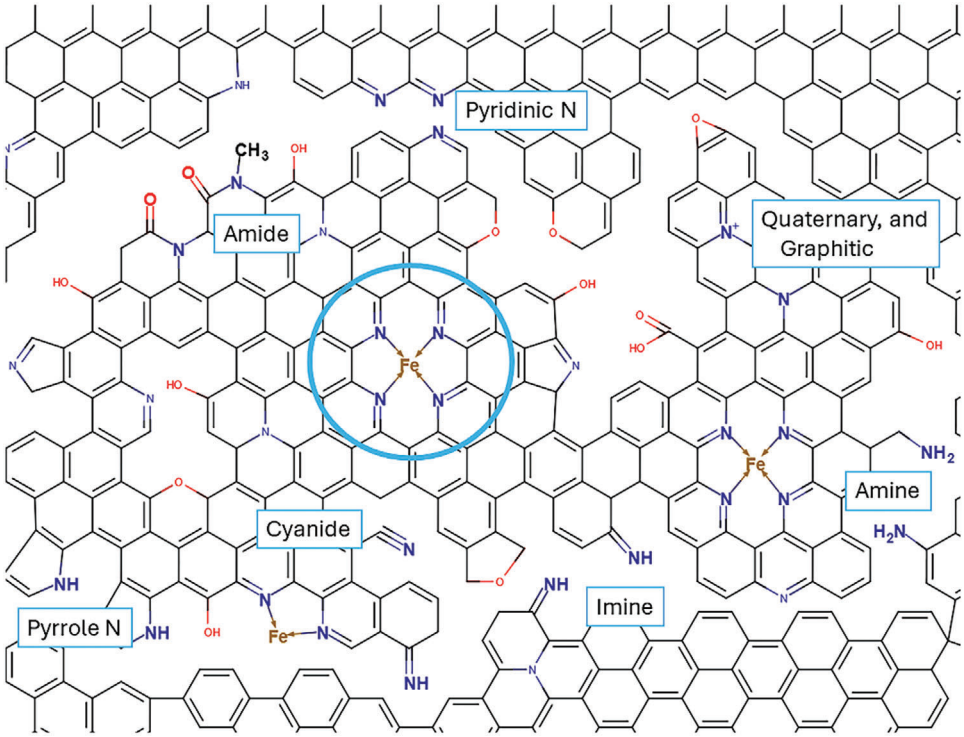

Figure 1. Schematic representation of the most important primary (MN_xC) and secondary (NC) sites within the chemical structure of a PGM-free electrocatalysts. A representative primary site (depicted as phthalocyanine- or porphyrin-like metal complexes embedded into a continuous carbon matrix) is highlighted while secondary sites (imine or cyanide groups, pyridinic N, amines or amides, pyrrolic (or protonated) N, graphitic N, and quaternary N) are labeled. Primary sites can have a variable number of N atoms ranging from 2 to 4.

C is mandatory since they must possess electronic conductivity along with intrinsic porosity, both required for electrocatalysis. Moreover, the heteroatoms inclusion creates a charge redistribution in the planes, influencing the catalytic performance.[7,14] The role of the metal is to create the primary active site for electrocatalysis. Indeed, the active sites are the coordination triad MN_xC (**Figure 1**), where M is the transition metal, N_x are multiple (from 2 to 4) atoms of N coordinating the metal, and C represents the carbon matrix they are incorporated within.[15] Among the transition metals, Fe-based PGM-free possess the highest catalytic activity toward the oxygen reduction reaction (ORR), durability, and scalability, making them attractive for practical applications in electrochemical devices.

Generally speaking, PGM-free for ORR can be synthesized from various organic and inorganic compounds,[16–19] but also from waste products.[20–24] This is mainly due to the synthesis methodology developed to maximize the catalytic efficiency, based on the mechanical mixing of compounds followed by one or more pyrolysis steps at high temperature and controlled atmosphere. The thermal treatment is usually above 900 °C in an inert atmosphere to increase material stability. Most of the processes also involve one or more acid washings to remove secondary unwanted phases and to create a porous structure.[15] Such secondary phases (oxides, carbides, nitrides, etc.) depend on the metal-containing compounds and are considered a byproduct of the pyrolysis step, actually decreasing the catalytic efficiency of the material.[15] In addition, metal-free secondary sites (NC) are always present in the form of C defects and N moieties,[15,25,26] as depicted in Figure 1. Compared to MN_xC sites, C defects and NC sites are catalytically less efficient producing the hydrogen peroxide byproduct, detrimental for the support.[27] Nevertheless, among NC sites pyridinic N are also useful for creating conjugation bonds with metallic ions forming the primary sites[15] and for the conversion of hydrogen peroxide into water.[28] It is thus straightforward that the maximization of pyridinic N is sought to improve the overall material efficiency.

In PGM-free literature, many approaches have been used for the synthesis of PGM-free but always relying on modified recipes of mixing, pyrolyzing, and postprocessing compounds, required to remove unwanted byproducts and ensure the appropriate stability. To maximize the pyridinic N, selected reagents have been used,[26,29] issuing a narrowing of the vastness of choice of precursors to a few compounds and hindering the affordability and cost-effectiveness of such materials. To address this problem, alternative approaches are mandatory. Among the known technologies for carbonaceous structure modification, ion beam techniques for selective ion implantation have been already investigated, both theoretically and experimentally, as desirable for large-scale production of fine-tuned semiconductors and optical-related materials, such as n- and p-doped graphene and C nanotubes.[30–39]

With the purpose of improving the PGM-free design, this study wants to investigate the feasibility of replicating the MN_xC coordination synthesis using a physics-based approach instead of the more common chemical route based on pyrolysis. The new

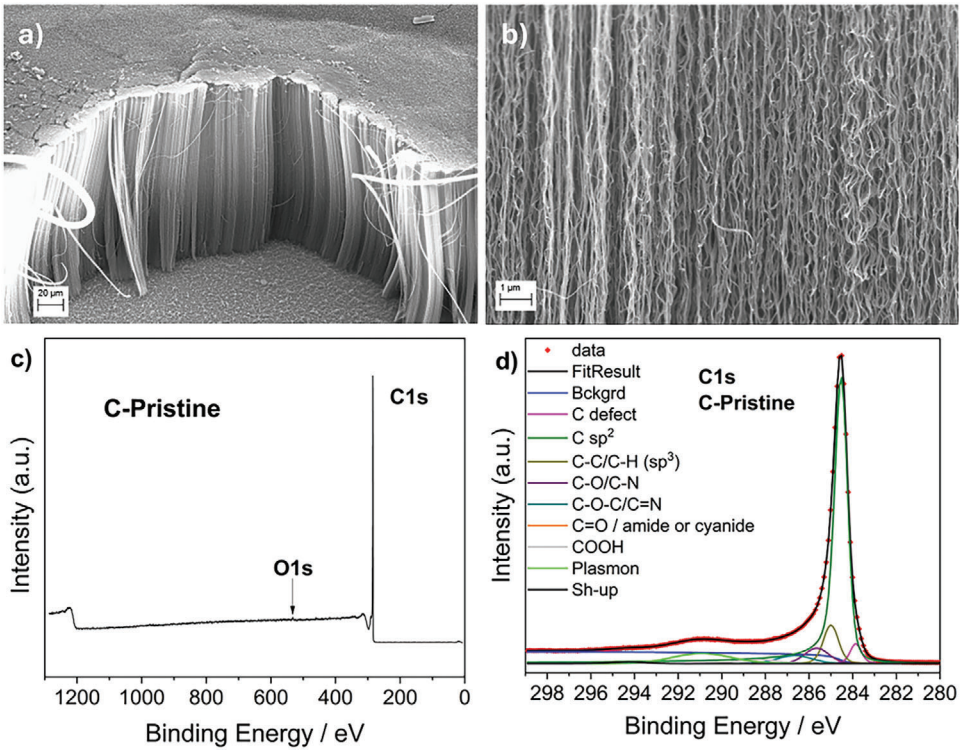

Figure 2. Characterization of pristine VA-CNT using different techniques; a) and b) SEM images of the supported VA-CNT; c) and d) XPS result of survey and C 1s core level showing the sp^2 characteristic nature of the sample.

synthesis methodology, entirely managed in a clean ultra-high-vacuum (UHV) chamber, relies on a N_2-fed Kaufman ion source for the nitrogen ion (N^+) implantation into a model C structure characterized by an almost total content of sp^2 carbon, obtained using vertically aligned carbon nanotubes (VA-CNT). Following this step, Fe evaporation using an electron beam evaporator is performed, to place over the material surface all the elements required to a PGM-free. The aim of the study is to investigate the possibility of maximizing the pyridinic nitrogen content by varying the ion beam energy and to evaluate the natural formation of MN_xC active sites under different synthesis conditions. Once fixed the proper recipe, the ultimate goal is to transpose the approach to other common and powder-like carbonaceous materials and obtain cleaner, fine-tuned PGM-free not depending on reagent compounds.

2. Results and Discussion

2.1. Characterization of the Model sp^2 C Material

To investigate the possibility of the natural formation of PGM-free active sites under different synthesis conditions, a two-step methodology is implemented: nitrogen implantation and iron evaporation. The N implantation into the carbonaceous support, meant as the backbone for the electrocatalyst, is preliminary performed using a model C structure characterized by an almost total content of sp^2 carbon, obtained using VA-CNT grown on rigid silicon supports. This is important because with a clean pristine material it is possible to minimize spurious contributions from intrinsic defects and other hybridizations that could impact the study. Once known the phenomena occurring in the model, the synthesis recipe can be extended and generalized to other common carbonaceous materials in the powder or woven form, more suitable for performance and real cell tests. Aiming at such a result, the supported VA-CNT were first investigated to collect data on control samples, using scanning electron microscopy (SEM), X-ray photoelectron spectroscopy (XPS), and Raman spectroscopy techniques to obtain morphological, compositional, and lattice dynamics (see further) information.

As reported in **Figure 2**, SEM of the as-grown pristine sample is characterized by a thick layer of VA-CNT of ≈150 – 200 µm in height, covering homogeneously the silicon support. The nanotubes are grouped into columnar structures holding together single units possessing a noodle-like shape (Figure 2a and b). The XPS chemical composition resulted only in two elements, with a complete predominance of carbon and very low amounts of oxygen. Within different batches, the oxygen content of the pristine material varied randomly between 0.6 and 14%, ascribable to samples' air exposure. The identified core levels were thus fitted, according to previous studies,[19,40–43] to obtain information on the chemical speciation. In the case of C 1*s*, in accordance with the literature,[30] the asymmetrical and sharp shape of the spectrum resulted in 71% of C sp^2 component (284.5 eV binding energy (BE), eV(BE)) and a total of ≈15% of defective bonds and sp^3 moieties (<284 eV(BE) and <286 eV(BE) respectively) with the remaining fraction referable to oxides (>286 eV(BE)).

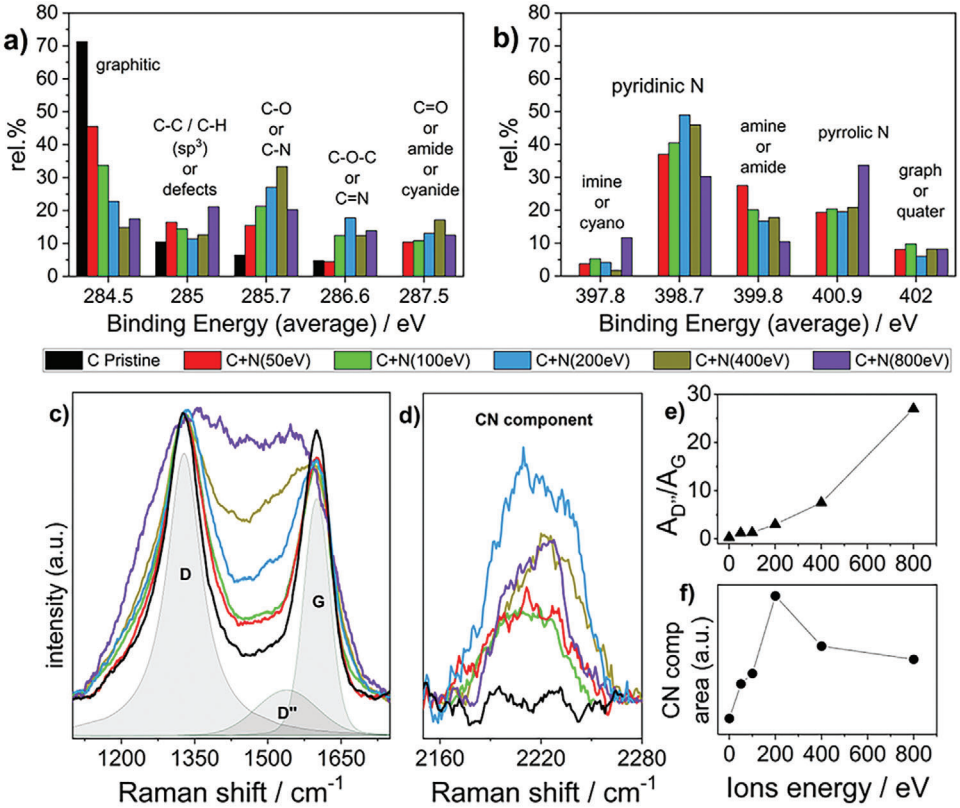

Figure 3. Summary of the surface functionalities of interest obtained from XPS upon nitrogenation of VA-CNT at different ion beam energies for a) C moieties and b) N moieties. c), d) Raman spectra collected in the *parallel to CNT* configuration in the 1100–1700 cm^{-1} and 2160–2280 cm^{-1} ranges at different ion beam energies. In panel c), the filled lines represent the fitting curves to the spectrum of the pristine sample (0 eV). e) Ratio between the areas of D'' and G peaks, $A_{D''}/A_G$, as a function of the ion beam energy. (f) Area of the band centered at 2220 cm^{-1} (shown in panel d) as a function of the ion beam energy.

2.2. Introducing N into the C Structure

To obtain a PGM-free electrocatalyst, the carbonaceous matrix should contain inclusions of nitrogen in order to create defects capable of allocating the single metal ions needed for the catalysis. Commonly, following the chemical route, based on high temperature pyrolysis, N inclusions into the carbon matrix are obtained by mixing the C support with N-containing compounds. In our case, nitrogen ions (N^+) are implanted into the C structure using a Kaufmann ion gun fed with pure N_2 gas. Among the device's parameters, namely, cathode current, discharge voltage, acceleration voltage, and ion beam energy, the latter was found to directly impact the nitrogen content and speciation. In the literature, ion beam energies below 100 eV have been used to implant and functionalize CNTs and graphene,[30,32,33] while higher energies in the range of tens of KeV were used to introduce defects in the carbon structure,[37,38] with ions passing through the nanotubes' walls. Moreover, nitrogen implantation into single and multiwalled CNTs was successfully achieved using energies between 50 and 300 eV,[31,34,35] with a displacement energy for an sp^2 C atom of ≈25–30 eV.[32,33] Based on this, five samples were prepared at different ion beam energies (50 eV, 100 eV, 200 eV, 400 eV, and 800 eV) and named accordingly. Above the highest value (800 eV), the N^+ ions energy is high enough to sputter the material surface, de facto posing an upper threshold for the parameter. After the treatment, XPS was repeated and integrated with Raman spectroscopy to understand the degree of modification of the carbon support. The XPS results of the element composition and chemical speciation are reported respectively in Tables S1 and S2 (Supporting Information) along with Figures S1–S3 (Supporting Information) for each core level. A summary of the mentioned Tables is depicted in **Figure 3**a,b.

Regarding the C core level, as can be seen from Figure S1 (Supporting Information), the increase in ion beam energy is correlated to a shape modification of the C 1*s* of the pristine sample, leading to a broadening of the spectra, but maintaining the typical asymmetrical profile. The monotonic increase in energy, from the 50 eV up to the 800 eV samples, was found to be associated with the surface graphitic content decrease from 70% down to 15% (Figure 3a), as expected by an ion treatment damaging the backbone structure of the VA-CNT. In addition, along with the diminishing of the C = C bond, defective (maximum for the 800 eV) and sp^3 structures are created, especially in the BE region commonly associated with oxides in the PGM-free literature (285.7 – 287.5 eV(BE)).[42–48] In this context, since the material is prepared in an uncontaminated chamber designed for ultra-high vacuum (UHV), but at a pressure of ≈10^{-4} mbar of pure N_2, it is very unlikely that the oxygen-containing moieties are increasing. This is further corroborated by the reduced or unmodified intensity of the O 1*s* peak after the sample exposure to

nitrogen ions (Figure S2, Supporting Information). Moreover, due to the similarities in the electronegativity of O and N, it is reasonable to conclude that the recorded increases in the C functionalities are instead associated with the introduction of N into the C matrix, creating stable bonds. Observing the trends (Figure 3a) and the broadening of the C 1*s* (Figure S1, Supporting Information), three different configurations, each at increasing BE of *ca* 1 eV, can be identified: single bond (C-N, ≈285.7 eV(BE)), double bonds (C = N, ≈286.6 eV(BE)), and triple bonds (amide or cyanide, ≈287.8 eV(BE)). As can be seen from Figure 3a, each configuration is characterized by a trend with a maximum corresponding to a certain N^+ ions energy. The single and triple bonds are maximized at the ion beam energy of 400 eV, with a relative maximum at 200 eV, while the C = N structure is augmented at 200 eV. It is important to stress that C = N is the one representing the pyridinic N functionality, the most important and sought-after in PGM-free electrocatalysts. Regarding N content, among the investigated ion beam energies, the 50 eV possesses the highest rate of inclusion with an N/C XPS signal ratio of 0.58 corresponding to 35.9 at%, while the 800 eV is the lowest with N/C of 0.24 (19.3 at%). In addition, a relative maximum was found again at 200 eV with a ratio of 0.38 (27.6 at%). In comparison with the typical PGM-free, the N amount is higher by at least a factor of 2. However, it is worth considering that XPS is a surface analysis, involving at most a few nanometers of the material external surface, hence below that limit of detection the N content could be different, but inaccessible by the technique. Based on such assumptions, it is reasonable to assert that the highest and lowest amounts of N are correlated with energies capable of pushing the N^+ ions too low or too deep within the material.

To better understand the carbon-nitrogen bond, N 1*s* core level was investigated in detail. Figure 3b and Figure S3 (Supporting Information) report respectively the summary of the chemical speciation and the N 1*s* spectra at the variation of the beam energy. The identified peaks were compatible with the literature of the chemical route synthesis.[28,34,40,48–50] Starting from the 50 eV sample, the spectrum shape possesses a main peak at BE of 399 eV with a shoulder at *ca* 401 eV(BE), becoming more evident for the samples 100 eV, 200 eV, and 400 eV. For the sample 800 eV, the spectrum shape changed into a two-component structure due to the increase of the peak at higher BE. From the literature of PGM-free,[28,43,49,51–56] the identified moieties are imine or cyano groups (≈397.8 eV(BE)), pyridinic N (≈398.7 eV(BE)), amine or amide groups (≈399.8 eV(BE)), pyrrolic or protonated N (≈400.9 eV(BE)), and graphitic or quaternary (N^+) (≈402 eV(BE)). Oxides can also be found at BE higher than 403 eV. The quantification of each functionality was found to be predominantly based on pyridinic N with a maximum of 49% for the sample 200 eV and a minimum of 30% for the 800 eV. The second main component, pyrrolic N, is constant ≈20% from the 50 to 400 eV samples, increasing to 33% for the 800 eV. Considering the importance of pyridinic moieties in PGM-free, as coordinators of metal ions but also as the only secondary sites capable of converting the hydrogen peroxide intermediate into water,[28] the reported data are peculiar of systems where the desired functionality is maximized. Moreover, among the prepared materials, the 200 eV sample possesses the highest amount of pyridinic N along with a minimized content of the remaining moieties, as can be seen in Figure 3b and Table S2 (Supporting Information).

To confirm the results of XPS, the lattice dynamics of pristine and nitrogenated samples were investigated by means of Raman with incident radiation in two configurations: *parallel* and *perpendicular* to CNT axis. This is meant to probe respectively the surface and the bulk of the samples. Further details and schematization are reported in the Supporting Information (Raman measurement of VA-CNT) and Figure S4 (Supporting Information). Regarding the surface, the results of the *parallel* configuration are reported in Figure 3c-f where two spectral regions are clearly visible (panels c and d), accounting respectively for the presence of disorder effects in the C matrix and CN vibrational activity. In the range 1100–1800 cm^{-1} (Figure 3c), with the increase of the ion beam energy, three phonon peaks are visibly changing, located at 1320, 1540, and 1600 cm^{-1} and assigned to D, D'' and G modes respectively. The G peak is associated with an in-plane displacement of the C atoms,[57,58] while D and D″ peaks are found when the disorder is introduced into the graphite structure. Moreover, in Figure 3d, the spectral region between 2150 and 2250 cm^{-1} is shown, hosting a quite broad and low-intensity band centered at 2200 cm^{-1}. Notably, this feature, whose central frequency is compatible with that expected for a cyanide stretching mode,[59] is evident only for samples exposed to nitrogen ions, while it completely lacks in pristine CNTs. This observation indicates that the presence and the intensity of the band reasonably bring information about the formation of CN bonds in the samples. Lastly, the band at 2200 cm^{-1} is consistent with the literature of Fe-based PGM-free synthesized with the standard chemical protocol and originated from the cyanide or nitrile bonds.[60,61] To quantify the modifications on the VA-CNT, the intensity ratio between D'' and G, $A_{D''}/A_G$, is reported in Figure 3e and provides an estimate of the degree of disorder in the system.[62] The progressive increase in the ratio between the areas of D'' and G, as a function of the ion beam energy indicates that the crystalline structure of the CNTs is progressively damaged as the nitrogenation process becomes more energetic. However, as shown in Figure 3f, the trend of the 2200 cm^{-1} band area as a function of the ion beam energy exhibits a maximum for the sample 200 eV, indicating a decorrelation between the degree of disorder in the lattice, as quantified by the $A_{D''}/A_G$ ratio, and the efficiency of the formation process of CN bonds.

Regarding the penetration depth of the nitrogen implantation, it was assessed by measuring the samples with incident radiation *perpendicular* to the CNT axis from the surface to the basis of CNTs. The spectra, reported in Figure S5 (Supporting Information), show that the band at 2220 cm^{-1}, remained visible also for measurements below the sample surface (0 µm) at a different extent depending on the ion beam energy. In addition, higher nitrogenating energy corresponded to deeper penetration along the CNT axis. This is clear evidence that the N implantation acts on a depth that goes far beyond the surface layer.

2.3. Fe Evaporation Over the N-Containing VACNTs

Based on previous XPS and Raman results, the 200-eV sample was selected as the reference material for further modifications. Indeed, inside the UHV chamber, the final step involved the introduction of metal ions over the nitrogenated samples.

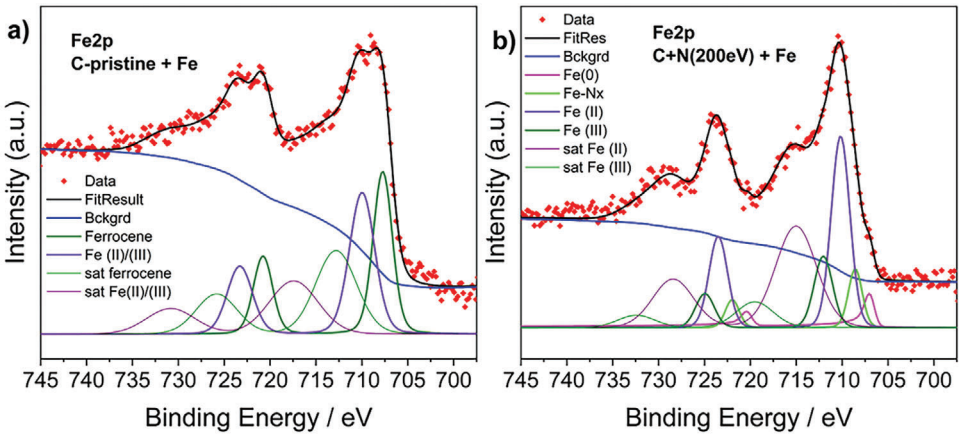

Figure 4. Results of the metalation of nitrogenated VA-CNT. XPS of a representative a) pristine sample (C-pristine + Fe) and b) nitrogenated C at 200 eV (C+N(200V) + Fe).

This is performed by deposition of the metal from an electron beam heated metallic target. The selected metal amount was chosen to be ≈0.1 nm, to minimize the aggregation and formation of (unwanted) secondary phases. Along with the sample containing the highest amount of pyridinic N (200 eV), a pristine sample not exposed to N was also prepared for comparison. The characterization methodology relied again on XPS and Raman analysis. The XPS results for N 1*s* and Fe 2*p* core levels are reported in **Figure 4** and Figure S6 (Supporting Information), respectively, and Raman results in Figure S7 (Supporting Information). The averaged element composition of samples before and after metalation is reported in Table S3 (Supporting Information) while the chemical speciation is in Tables S4 and S5 (Supporting Information). Regarding the Fe content, it was found to be ≈0.7 ± 0.1 at.% and 0.9 ± 0.2 at.%, respectively for pristine and nitrogenated samples and consistent with the PGM-free literature.[19,24,45,63] The N 1*s* spectra of all the 200 eV samples, before and after iron deposition (Figure S6, Supporting Information) showed clearly observable differences in shape with respect to the as-prepared ones (Figure S3c, Supporting Information). The discrepancies could be explained in terms of a reorganization of the metastable implanted systems[31] upon exposure to air. However, no increase in oxide components was observed, meaning that some less stable N moieties could have reorganized in more stable configurations. With respect to the spectrum of the as-synthesized sample (Figure S3c, Supporting Information), the amine/amide component increased, pyrrolic decreased, and the pyridinic content also slightly decreased. In any case, pyridinic N was found to be the major component with an average content of 42.5 ± 1.7 rel.% (Table S4, Supporting Information). Along with these differences, upon Fe deposition the spectra resulted upshifted of ≈0.2 – 0.3 eV(BE) with respect to the unmetalated ones (Figure S6e, Supporting Information), indicating the presence of a modification of the spectra. It is thus straightforward to think about the introduction of the N_x-Fe coordination that is at the basis of the PGM-free catalytic activity. However, the fitting of N 1*s* resulted in a certain degree of uncertainty due to the superposition of amine contributions with the N_x-Fe fraction representative of the active site formation.[28,55] The fit was thus performed constraining all the parameters of the original fit of unmetalated samples (Figure S6c, Supporting Information) and adding an additional component between 399.5 – 399.8 eV(BE) followed by a relaxation only on the peak's intensity (Figure S6d, Supporting Information). The hypothesized N_x-Fe component was thus roughly evaluated in the amount of 13 ± 4 rel.% followed by a decrease in imine / cyano, pyridinic, and amine / amide groups (Figure S6f, Supporting Information). The quantified data have been summarized in Table S4 (Supporting Information).

Nevertheless, the validation of the PGM-free active sites' formation came from the Fe2p core levels reported in Figure 4a and b. The metalated pristine (Figure 4a) and nitrogenated (Figure 4b) samples possess differences in the spectrum shape with a main broad line that is actually deconvoluted into two main components (707.7 ± 0.1 eV(BE) and 709.9 ± 0.1 eV(BE)) for the pristine and just one main line (710.2 ± 0.2 eV(BE)), with minor contributions in the nitrogenated one. Upon full deconvolution, the metalated pristine samples were found to show similarities with a mixed valence Fe_3O_4 spectrum[64,65] but with a spin-orbit splitting of 13 eV(BE) typical of metallic iron. However, to fit the sample spectra, a two-component satellite structure was required. The first was located at 712.7 ± 0.3 eV(BE) while the other was at 717.0 ± 0.4 eV(BE). The latter can be easily associated with mixed Fe(II)/Fe(III) compounds, but the former has no meaning if a metallic structure is present, since Fe(0) is known to possess no satellites. Moreover, the line located at 707.7 eV(BE) is upshifted by at least 0.6 eV(BE) with respect to Fe(0). However, by associating such a line with the satellite component at 712.7 eV(BE) it is possible to identify a ferrocene-like compound, where Fe is coordinated to π-conjugated carbonaceous structures, as reported in the literature.[66–69]

Moving to the nitrogenated samples, the spectra shape was found more similar to the FeO with the characteristic satellite ≈715 eV(BE), peculiar to the Fe(II) compounds (Figure 4b).[70–73] However, to complete the fit it was necessary to insert a small fraction of metallic Fe and a certain degree of higher oxidation (Fe(III)) with a component at 712.1 ± 0.4 eV(BE) and the characteristic satellite at 719.1 ± 1.0 eV(BE). Lastly, more importantly, the validation of the presence of Fe-N_x active sites was found with a line located at 708.7 ± 0.2 eV(BE), consistent with the PGM-free

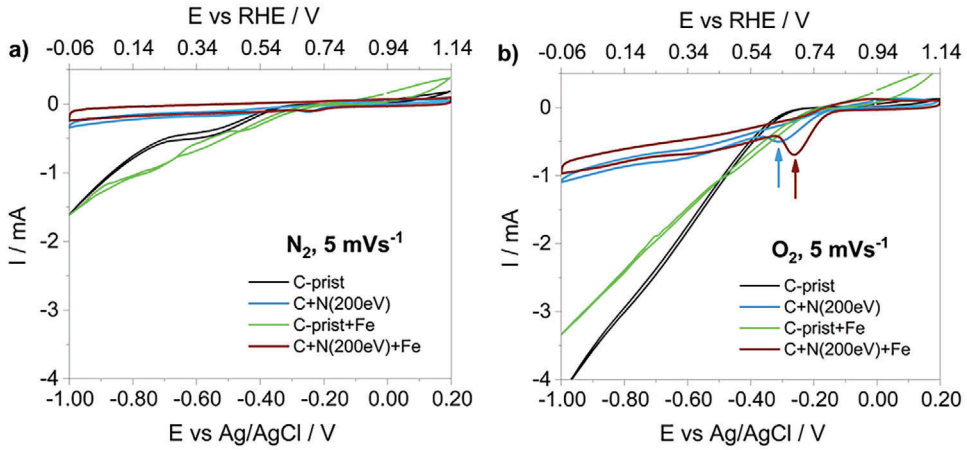

Figure 5. CV results @ 5 mVs^{-1} in a narrow range scan of 1.2 V in 0.1M KOH purged with a) N_2 and b) O_2 of C-pristine, C+N(200eV), C-pristine + Fe, and C+N(200eV) + Fe. Characteristic ORR activity is clearly visible and highlighted by arrows. The RHE scale reported at the top of the graphs is calibrated with the hydrogen reduction/oxidation method (Figure S8, Supporting Information).

literature[24,28,49,51] and quantified in 12.4 ± 3.8 rel.%. The presence of no satellites associated with the Fe-N_x contribution led to the conclusion that the metal could be coordinated in a low-spin Fe^{2+} configuration.[71]

Interestingly, the deposition of Fe over pristine and nitrogenated samples did not affect the lattice dynamics. In Figure S7 (Supporting Information) are shown the 1100–1800 cm^{-1} bands for the same samples investigated using XPS. As can be seen, the spectra almost completely overlapped in the D and G bands, with just lesser modifications of the D'' band of the 200 eV, eventually due to the formation of the Fe-N_x active sites.

2.4. Electrochemical Characterization

The electrocatalytic behavior toward the oxygen reduction reaction (ORR) of the as-synthesized materials was tested in a three electrodes setup using the cyclic voltammetry (CV) method. At this stage, no additional tests can be performed on these systems, since the samples are prepared over one of the two faces of a 1 × 1 cm^2 oxide-covered Si support, referring to future papers for additional characterization based on hydrodynamic conditions. Before testing the ORR ability, a Reversible Hydrogen Electrode (RHE) calibration (Figure S8, Supporting Information) was performed. In addition, a complete analysis of the support was done, both in N_2 and O_2 purging atmospheres, to avoid contributions in the ORR potential window (1 – 0 V vs. RHE) originating from the side of the support in contact with the electrolyte solution. As can be seen from the scans reported in Figure S9a (Supporting Information), the support did not influence the electrochemistry, possessing characteristic faradaic peaks at potentials higher than 1.0 V versus RHE. Moreover, shortening the upper potential range from 1.34 V versus RHE to 1.14 V versus RHE led to the disappearance of such features (Figure S9b, Supporting Information). In any case, the registered total current of the smooth supports was in the range of μA while the VA-CNT samples showed a capacitive current in the mA range, influenced by the presence of oxygen. The characteristic electrocatalytic behavior of the samples in 0.1 M KOH solution is reported in **Figure 5**, with background scans (N_2-purged solution) in Figure 5a and ORR activity (O_2-purged solution) in Figure 5b. Starting from the pristine sample (C-prist, black lines), the CV showed an ohmic current-potential (I-V) curve with onset at ≈0.7 V versus RHE, very similar to the control sample without nitrogen (C-prist+Fe, light green lines). This is mostly due to the hydrophobic nature of the samples. However, the introduction of nitrogen followed by iron evaporation implemented the ORR ability of the system. In the case of C+N(200eV) (light blue lines), nitrogen implantation changed the I-V behavior from pure ohmic to standard capacitive, due to the induced hydrophilicity, with the presence of a faradaic contribution clearly visible at the potential versus RHE of 0.62 V, compatible with the contribution of carbonaceous support of PGM and PGM-free.[74] Such a peak, identified by the light blue arrow, possesses a current of -0.51 mA. Furthermore, the Fe evaporation and the creation of Fe-N_x coordination, as shown in the XPS section, implemented the capacitive current but also upshifted the reduction peak (C+N(200eV)+Fe, wine lines and arrow) to a potential of 0.68 V versus RHE with a reduction current of -0.69 mA. For the sake of completeness, in N_2 purged electrolyte both N-containing samples showed a residual faradaic activity (≈ −0.1 mA) that can be reconducted to ORR of oxygen trapped within the intrinsic porosity created by the VA-CNT, that eventually needed longer CV cycling to be removed.

3. Considerations and Future Perspectives

The choice of VACNT prepared with the chemical vapor deposition (CVD) technique as the starting material for this study was a priority to set up an uncontaminated C model. The VA-CNT are a geometrically ordered sp^2 C structure in which CNTs morphological/structural features can be controlled through a precise tuning of CVD process parameters (i.e., reaction temperature, gas pressure and flow rate, and size of the growth seeds). VA-CNTs are required to investigate the changes occurring in the system upon N implantation and Fe-N_x sites formation on the basis of the spectroscopic experience developed on standard PGM-free. However, in the long run, such a choice became detrimental

considering the common approaches used for the electrochemical characterization of new electrocatalysts. The VA-CNT system has limited electrochemical performances that are not comparable with the most active of PGM-free.[75–78] To explain such results, the peculiarity of this model system is to study the feasibility of a new synthesis method must be considered. The Si support used for the VA-CNT growth possesses an electric conductivity much lower than the standard glassy carbon used in conventional benchmarks. In addition, the VA-CNTs have modifications exerted only on the external surface, de facto ignoring the whole porosity of the system and the high surface area of such nanomaterial. Moreover, the electrocatalytic behavior can be also ascribed to low-spin ferrous active sites coordinated to pyridinic N, which have been identified as lesser sites for ORR, being held in defects not located directly in the C sp^2 plane,[27,56,79] but more durable compared to high-spin ferric ones.[80] The creation of those sites can be reconducted again to the geometry of the system, with VA-CNT length oriented parallel to the nitrogen ion beam. At this stage, the removal of the nanotubes layer from the Si support did not lead to the possibility of obtaining a catalytic ink to be used in hydrodynamic tests for electrochemical benchmarking (RRDE). The result was a debundled mass of C nanotubes covering the signal of the Fe-N_x sites created on the topmost external surface of VA-CNTs. Nevertheless, the methodology can be directly implemented over woven forms of carbon-like fibers or felts with the final intent to obtain a 2D material ready to be used as electrodes in real cell tests. Regarding the possibility of using powder compounds like commercial CNTs, a setup implementation would be required. A more reasonable approach (but time- and cost-demanding) would have been the synthesis exerted with a specifically designed setup capable of moving a pure powder-like C-containing material during the Fe evaporation step. However, despite such flaws, the result is clear evidence of the incremented catalytic activity of the N+Fe-containing material prepared for the first time with a route different from the chemical one. If properly rationalized, the implantation method approach could pave the way to future implementation of the methodology, requiring only nitrogen gas for the formation of N-containing C supports for PGM-free. Lastly, the metal evaporation step is not constrained only to Fe but open to a plethora of noble and non-noble transition metals that can be, in principle, combined at will. By changing the metal and selecting an appropriate carbon support, different catalytic reactions could be catalyzed.

4. Conclusions

The feasibility of a new methodology based on non-chemical modifications of sp^2 C structure for the synthesis of PGM-free based on Fe was assessed in a case study through XPS, Raman, and electrochemistry. Upon selecting an appropriate C allotrope as a model material (vertically aligned carbon nanotubes) that helped in the minimization of contributions not originating from pure graphitic C, a nitrogen-compound-free material can be prepared, leading to a synthesis recipe intended to be extended to common powder-like C structures. Using nitrogen ion implantation with appropriate beam energy by means of a Kaufman ion source fed on N_2 gas and Fe evaporation inside an UHV chamber, it was possible to obtain similar results, in terms of surface chemistry, as the chemical route based on mixing, pyrolyzing, and post-processing of reagents. The creation of direct bonding of implanted N with the C support and later the formation of the metal-containing active sites was demonstrated, by XPS and Raman, outside the established chemical methodology based on high-temperature pyrolysis. Moreover, the maximization of pyridinic N moieties can be obtained, of paramount importance for the stabilization of Fe-N_x active sites, lacking in the control sample without N. This led, for the first time with physics methodology, to electrochemically active materials showing clear improvements in the electrocatalysis of oxygen with respect to the unmodified samples. If properly implemented, the established approach is thus promising for the preparation of N-compound-free electrocatalysts for energy-related reactions without involving aggressive and time-consuming post-treatments, paving the way for interesting possibilities in the continuous improvement of PGM-free.

5. Experimental Section

Samples Preparation: *VA-CNT Synthesis*: VA-CNTs were directly synthesized over silicon growth substrates at the Sapienza-INFN TITAN laboratory by employing a customized and high-vacuum chemical vapor deposition (CVD) chamber with a base pressure in the low 10^{-7} mbar range. The CVD process used for the growth of VA-CNTs is based on the decomposition of acetylene (carbon precursor) which is catalyzed by iron nanoparticles, as described elsewhere.[81–84] Briefly, boron-doped <100> Si wafers, with 1000 nm of thermally grown silicon dioxide, were cleaved into 40 mm × 20 mm strips and cleaned via the Radio Corporation of America method. A thin (3 nm in thickness) catalyst layer of iron was deposited by means of electron beam evaporation over these Si-based strips which were, subsequently, mounted on the heating element of the CVD reaction chamber. To promote the formation of iron nanoparticles, here acting as growth seeds for CNTs, an annealing treatment was performed at 720 °C in a reducing H_2-atmosphere for 4 min. After this pre-synthesis annealing step, acetylene was injected in the CVD reactor and the sample temperature was increased to 740 °C, running the growth for 10 min. Finally, the sample temperature was reduced to room temperature under the base pressure of the CVD system. The process parameters used for the synthesis of VA-CNTs rely on our previous work.[83]

PGM-free Preparation: Nitrogen Implantation: Nitrogen ion implantation on VA-CNT samples was conducted at the Spectro-Microscopy laboratory (SMART) of the Department of Physics of Sapienza University of Rome and was made by means of a DC cathode ion beam source (Kaufman ion source) supplied by Plasma Process Group Inc. and fed with pure nitrogen (titrated 5.0). Appropriate parameters have been set to get ionization in the plasma cavity, whose stability has been guaranteed by means of a fine-tuning of the gas flow through a leak valve ($P = 2 \times 10^{-4}$ mbar in the vacuum chamber) while monitoring the nitrogen partial pressure in the UHV chamber. The VA-CNT samples underwent a 20 min exposition to the N^+ ions, with a cathode current of 3.1 A, a discharge voltage of 80 V, and an accelerating voltage of 85 V, varying the beam energy for each one, specifically 50, 100, 200, 400, and 800 eV, to explore the effect of ions landing energy in terms of induced defects, bonding sites, and penetration depth of implantation. No sample annealing has been performed. The samples were labeled according to the implantation energy.

PGM-free Preparation: Iron Evaporation: Iron evaporation was conducted at the molecular beam epitaxy (MBE) facility of the Department of Physics of Politecnico di Milano. The samples were placed inside an ultra-high vacuum (UHV) chamber (base pressure in 10^{-11} mbar) where an electron beam (e-beam) cell filled with Fe rod allowed the deposition of small amounts of iron on the samples. The iron flux was monitored by a quartz microbalance and an overall amount of ≈0.1 nm was deposited on each sample.

Samples Characterization: *SEM Characterization*: The morphological characterization was exerted through a Zeiss Auriga scanning electron microscopy (SEM) operating at an accelerating voltage of 15 kV.

XPS Characterization: The chemical speciation and elemental composition were investigated using X-ray photoelectron spectroscopy (XPS) analysis in UHV in two different laboratories due to the lack of both Kaufman ion source and e-beam evaporator on the same XPS apparatus. At Sapienza University, to investigate the samples before and after N implantation using a SPECS PHOIBOS 150 XPS system equipped with a monochromatic Al K_α (1486.6 eV) X-ray source and high-speed imaging 2D CMOS true counting detector. At Politecnico di Milano, to characterize the sample before and after the Fe deposition, using the same analyzer model and a non-monochromatic Al source. The systems were calibrated using Au4f core level at 83.95 eV. Full survey scans and C1s, O1s, N1s, and Fe2p core levels were investigated for each sample. The fittings were performed using Kalibri KolXPD software.

Raman Characterization: The analysis of the lattice dynamics was conducted using Raman spectroscopy in two different laboratories. The measurements before and after N implantation were carried out at Sapienza University at room temperature by a Horiba LabRAM HR Evolution microspectrometer, operating in backscattering geometry, coupled with a 600 grooves mm^{-1} diffraction grating and a Peltier-cooled charge-coupled device (CCD) detector. The employed light source was a 632.8 nm He-Ne laser focused on the sample by a microscope equipped with objectives of different magnification. For further details see.[85] The spectra were collected in two distinct configurations: i) with a 4x objective, orienting the sample with the CNT axis parallel to the propagation direction of the incident radiation, to get information about the average characteristics of the sample surface (*parallel configuration*), and ii) with a 100x objective, orienting the sample with the CNT axis perpendicular to the propagation direction of the incident radiation, to investigate the evolution of the Raman peaks moving from the surface to the bottom of the CNTs (*perpendicular configuration*). The measurements before and after Fe evaporation were carried out at Politecnico di Milano with a Horiba LabRAM HR 800, operating in the same geometry with the same diffraction grating, detector, and light source. The spectra were collected with a 50x NA 0.75 objective, orienting the sample with the CNT axis parallel to the propagation direction of the incident radiation.

Electrochemistry Characterization: The electrochemical tests were performed in 0.1 M KOH using a three electrodes setup with an Ag/AgCl reference electrode (Equilabrium RRPEAGCL-EQ) and a graphite rod as the counter electrode. The samples grown and modified over the doped silicon support with 1000 nm thick oxide layer were used as working electrodes. The electrocatalytic properties, both in N_2 and O_2, were tested using the Cyclic Voltammetry technique through a pocket PalmSense 4 potentiostat. The potentials recorded versus Ag/AgCl were converted versus Reversible Hydrogen Electrode (RHE) upon calibration of the reference by measuring the change from hydrogen evolution to hydrogen oxidation at 1 mV s^{-1} in H_2-saturated electrolyte using a platinum foil as the working electrode and gold wire as the counter electrode.

Statistical Analysis: For the purposes of this study, a total of 33 samples have been prepared and tested, managing between three and five replicates for each sample considered in the main text. Each sample's size was $\approx$1 cm^2. All the presented data, if otherwise stated, were in the format of mean value $\pm$ standard deviation (mean $\pm$ SD).

Supporting Information

Supporting Information is available from the Wiley Online Library or from the author.

Acknowledgements

The Authors were thankful to Dr. Francesco Mura of CNIS Sapienza for the SEM images. The Authors were thankful to Prof. Paolo Postorino for his assistance in the Raman investigation. VCAF was thankful to Marco Menegazzo for his assistance during the measurement sessions at Politecnico di Milano. VCAF was thankful to Prof. Maria Assunta Navarra for the hospitality in her electrochemistry laboratory. The experiments (XPS, Raman) were partially or totally (Kaufman exposure) carried out at the SmartLab departmental laboratory of the Department of Physics at Sapienza University of Rome. VCAF and EP acknowledge funding from the European Union – NextGenerationEU under the National Recovery and Resilience Plan (NRRP), Mission 4, Component 2 Investment 1.3 – Call for tender No. 1561 of 11.10.2022 of Ministero dell'Università e della Ricerca (MUR) Project code PE0000021, Concession Decree No. 1561 of 11.10.2022, CUP B53C22004070006; Project title "Network 4 Energy Sustainable Transition – NEST". FP, IR, and GC acknowledge the italian Ministero Università e Ricerca (MUR) under the PRIN grant "ANDROMeDA" (PRIN_2020Y2JMP5) and the ATTRACT project funded by the EC under Grant Agreement 777 222. VCAF acknowledges Chemaxon for the use of Marvin software suite.

Conflict of Interest

The authors declare no conflict of interest.

Author Contributions

V.C.A.F. performed methodology, investigation, conceptualization, data curation, visualization, wrote the original draft. M.S. performed methodology, investigation, wrote, reviewed and edited. E.S. performed methodology, investigation, wrote, reviewed and edited. I.R. performed methodology, investigation, wrote, reviewed and edited. F.G. performed methodology and investigation. I.M. performed methodology and investigation. G.C. performed methodology, investigation, wrote, reviewed and edited. F.P. performed methodology and investigation. A.C. performed methodology and investigation. A.L. performed methodology and investigation. G.B. performed methodology, investigation, conceptualization, resources, wrote, reviewed and edited. E.P. performed methodology, investigation, conceptualization, resources, wrote, reviewed and edited, supervision, project administration, and funding acquisition.

Data Availability Statement

The data that support the findings of this study are available from the corresponding author upon reasonable request.

Keywords

aligned CNT, ion implantation, nanomaterials, PGM-free, Raman, XPS

Received: July 24, 2024
Revised: November 21, 2024
Published online:

[1] N. M. Marković, P. N. Ross, *Surf. Sci. Rep.* **2002**, *45*, 117.
[2] B. C. H. Steele, A. Heinzel, *Nature* **2001**, *414*, 345.
[3] S. Chu, A. Majumdar, *Nature* **2012**, *488*, 294.
[4] A. S. Aricò, P. Bruce, B. Scrosati, J.-M. Tarascon, W. van Schalkwijk, *Nat. Mater.* **2005**, *4*, 366.
[5] U. Martinez, S. Komini Babu, E. F. Holby, H. T. Chung, X. Yin, P. Zelenay, *Adv. Mater.* **2019**, *31*, 1806545.
[6] C. Santoro, A. Lavacchi, P. Mustarelli, V. Di Noto, L. Elbaz, D. R. Dekel, F. Jaouen, *ChemSusChem* **2022**, *15*, 202200027.

[7] A. Li, S. A. Nicolae, M. Qiao, K. Preuss, P. A. Szilágyi, A. Moores, M.-M. Titirici, *ChemCatChem* **2019**, *11*, 3602.
[8] W. Moschkowitsch, O. Lori, L. Elbaz, *ACS Catal.* **2022**, *12*, 1082.
[9] Y. Li, H. Wang, C. Priest, S. Li, P. Xu, G. Wu, *Adv. Mater.* **2021**, *33*, 2000381.
[10] Y. He, G. Wu, *Acc. Mater. Res.* **2022**, *3*, 224.
[11] Z. Chen, X. Zhang, W. Liu, M. Jiao, K. Mou, X. Zhang, L. Liu, *Energy Environ. Sci.* **2021**, *14*, 2349.
[12] V. C. A. Ficca, C. Santoro, E. Marsili, W. da Silva Freitas, A. Serov, P. Atanassov, B. Mecheri, *Electrochim. Acta* **2022**, *402*, 139514.
[13] V. C. A. Ficca, C. Santoro, A. D'Epifanio, S. Licoccia, A. Serov, P. Atanassov, B. Mecheri, *ChemElectroChem* **2020**, *7*, 3044.
[14] A. Sarapuu, E. Kibena-Põldsepp, M. Borghei, K. Tammeveski, *J. Mater. Chem. A* **2018**, *6*, 776.
[15] T. Asset, P. Atanassov, *Joule* **2020**, *4*, 33.
[16] U. Martinez, E. F. Holby, S. K. Babu, K. Artyushkova, L. Lin, S. Choudhury, G. M. Purdy, P. Zelenay, *J. Electrochem. Soc.* **2019**, *166*, F3136.
[17] M. A. C. de Oliveira, V. C. A. Ficca, R. Gokhale, C. Santoro, B. Mecheri, A. D'Epifanio, S. Licoccia, P. Atanassov, *J. Solid State Electrochem.* **2021**, *25*, 93.
[18] W. Moschkowitsch, S. Gonen, K. Dhaka, N. Zion, H. Honig, Y. Tsur, M. Caspary-Toroker, L. Elbaz, *Nanoscale* **2021**, *13*, 4576.
[19] B. Mecheri, V. C. A. Ficca, M. A. Costa de Oliveira, A. D'Epifanio, E. Placidi, F. Arciprete, S. Licoccia, *Appl. Catal. B Environ.* **2018**, *237*, 699.
[20] S. A. Mirshokraee, M. Muhyuddin, R. Lorenzi, G. Tseberlidis, C. L. Vecchio, V. Baglio, E. Berretti, A. Lavacchi, C. Santoro, *SusMat* **2023**, *3*, 248.
[21] S. Zago, M. Bartoli, M. Muhyuddin, G. M. Vanacore, P. Jagdale, A. Tagliaferro, C. Santoro, S. Specchia, *Electrochim. Acta* **2022**, *412*, 140128.
[22] S. A. Mirshokraee, M. Muhyuddin, R. Morina, L. Poggini, E. Berretti, M. Bellini, A. Lavacchi, C. Ferrara, C. Santoro, *J. Power Sources* **2023**, *557*, 232571.
[23] M. Muhyuddin, J. Filippi, L. Zoia, S. Bonizzoni, R. Lorenzi, E. Berretti, L. Capozzoli, M. Bellini, C. Ferrara, A. Lavacchi, C. Santoro, *ChemSusChem* **2022**, *15*, 202102351.
[24] G. Zuccante, M. Muhyuddin, V. C. A. Ficca, E. Placidi, M. Acciarri, N. Lamanna, A. Franzetti, L. Zoia, M. Bellini, E. Berretti, A. Lavacchi, C. Santoro, *ChemElectroChem n/a*, 202300725.
[25] C. V. Rao, C. R. Cabrera, Y. Ishikawa, *J. Phys. Chem. Lett.* **2010**, *1*, 2622.
[26] S. Yasuda, L. Yu, J. Kim, K. Murakoshi, *Chem. Commun.* **2013**, *49*, 9627.
[27] S. Specchia, P. Atanassov, J. H. Zagal, *Curr. Opin. Electrochem.* **2021**, *27*, 100687.
[28] K. Artyushkova, A. Serov, S. Rojas-Carbonell, P. Atanassov, *J. Phys. Chem. C* **2015**, *119*, 25917.
[29] J. H. Dumont, U. Martinez, K. Artyushkova, G. M. Purdy, A. M. Dattelbaum, P. Zelenay, A. Mohite, P. Atanassov, G. Gupta, *ACS Appl. Nano Mater.* **2019**, *2*, 1675.
[30] B. Ni, R. Andrews, D. Jacques, D. Qian, M. B. J. Wijesundara, Y. Choi, L. Hanley, S. B. Sinnott, *J. Phys. Chem. B* **2001**, *105*, 12719.
[31] J. Kotakoski, A. V. Krasheninnikov, Y. Ma, A. S. Foster, K. Nordlund, R. M. Nieminen, *Phys. Rev. B* **2005**, *71*, 205408.
[32] T. Kamimura, K. Yamamoto, T. Kawai, K. Matsumoto, *Jpn. J. Appl. Phys.* **2005**, *44*, 8237.
[33] K. Yamamoto, T. Kamimura, K. Matsumoto, *Jpn. J. Appl. Phys.* **2005**, *44*, 1611.
[34] F. Xu, M. Minniti, P. Barone, A. Sindona, A. Bonanno, A. Oliva, *Carbon* **2008**, *46*, 1489.
[35] U. Bangert, A. Bleloch, M. H. Gass, A. Seepujak, J. van den Berg, *Phys. Rev. B* **2010**, *81*, 245423.
[36] S. Garaj, W. Hubbard, J. A. Golovchenko, *Appl. Phys. Lett.* **2010**, *97*, 183103.
[37] B. Guo, Q. Liu, E. Chen, H. Zhu, L. Fang, J. R. Gong, *Nano Lett.* **2010**, *10*, 4975.
[38] A. Ishaq, S. Iqbal, N. Ali, A. A. Khurram, A. U. Akrajas, C. F. Dee, S. Naseem, H. M. Rafique, Y. Long, *New Carbon Mater* **2013**, *28*, 81.
[39] T. Granzier-Nakajima, K. Fujisawa, V. Anil, M. Terrones, Y.-T. Yeh, *Nanomaterials* **2019**, *9*, 425.
[40] B. Ricciardi, W. da Silva Freitas, B. Mecheri, K. U. Nisa, J. Montero, V. C. A. Ficca, E. Placidi, C. Alegre, A. D'Epifanio, *Carbon* **2024**, *219*, 118781.
[41] W. da Silva Freitas, B. Mecheri, C. Lo Vecchio, I. Gatto, V. Baglio, V. C. A. Ficca, A. Patra, E. Placidi, A. D'Epifanio, *J. Power Sources* **2022**, *550*, 232135.
[42] M. Smith, L. Scudiero, J. Espinal, J.-S. McEwen, M. Garcia-Perez, *Carbon* **2016**, *110*, 155.
[43] K. Artyushkova, S. Rojas-Carbonell, C. Santoro, E. Weiler, A. Serov, R. Awais, R. R. Gokhale, P. Atanassov, *ACS Appl. Energy Mater.* **2019**, *2*, 5406.
[44] V. C. A. Ficca, C. Santoro, E. Placidi, F. Arciprete, A. Serov, P. Atanassov, B. Mecheri, *ACS Catal.* **2023**, *13*, 2162.
[45] W. da Silva Freitas, A. D'Epifanio, V. C. A. Ficca, E. Placidi, F. Arciprete, B. Mecheri, *Electrochim. Acta* **2021**, *391*, 138899.
[46] H. L. Poh, P. Šimek, Z. Sofer, M. Pumera, *ACS Nano* **2013**, *7*, 5262.
[47] R. Gokhale, Y. Chen, A. Serov, K. Artyushkova, P. Atanassov, *Electrochim. Acta* **2017**, *224*, 49.
[48] Y. He, H. Guo, S. Hwang, X. Yang, Z. He, J. Braaten, S. Karakalos, W. Shan, M. Wang, H. Zhou, Z. Feng, K. L. More, G. Wang, D. Su, D. A. Cullen, L. Fei, S. Litster, G. Wu, *Adv. Mater.* **2020**, *32*, 2003577.
[49] K. Artyushkova, C. Walker, W. Patterson, P. Atanassov, *Electrocatalysis* **2014**, *5*, 241.
[50] X. Yin, H. T. Chung, U. Martinez, L. Lin, K. Artyushkova, P. Zelenay, *J. Electrochem. Soc.* **2019**, *166*, F3240.
[51] W. da Silva Freitas, A. D'Epifanio, C. Lo Vecchio, I. Gatto, V. Baglio, V. C. A. Ficca, E. Placidi, B. Mecheri, *Chem. Eng. J.* **2023**, *465*, 142987.
[52] B. Ricciardi, B. Mecheri, W. da Silva Freitas, V. C. A. Ficca, E. Placidi, I. Gatto, A. Carbone, A. Capasso, A. D'Epifanio, *ChemElectroChem* **2023**, *10*, 202201115.
[53] I. Matanovic, K. Artyushkova, P. Atanassov, *Curr. Opin. Electrochem.* **2018**, *9*, 137.
[54] I. Matanovic, K. Artyushkova, M. B. Strand, M. J. Dzara, S. Pylypenko, P. Atanassov, *J. Phys. Chem. C* **2016**, *120*, 29225.
[55] K. Artyushkova, I. Matanovic, B. Halevi, P. Atanassov, *J. Phys. Chem. C* **2017**, *121*, 2836.
[56] M. Primbs, Y. Sun, A. Roy, D. Malko, A. Mehmood, M.-T. Sougrati, P.-Y. Blanchard, G. Granozzi, T. Kosmala, G. Daniel, P. Atanassov, J. Sharman, C. Durante, A. Kucernak, D. Jones, F. Jaouen, P. Strasser, *Energy Environ. Sci.* **2020**, *13*, 2480.
[57] L. Graziotto, F. Macheda, T. Venanzi, G. Marchese, S. Sotgiu, T. Ouaj, E. Stellino, C. Fasolato, P. Postorino, M. Metzelaars, P. Kögerler, B. Beschoten, M. Calandra, M. Ortolani, C. Stampfer, F. Mauri, L. Baldassarre, *Nano Lett.* **2024**, *24*, 1867.
[58] T. Venanzi, L. Graziotto, F. Macheda, S. Sotgiu, T. Ouaj, E. Stellino, C. Fasolato, P. Postorino, V. Mišeikis, M. Metzelaars, P. Kögerler, B. Beschoten, C. Coletti, S. Roddaro, M. Calandra, M. Ortolani, C. Stampfer, F. Mauri, L. Baldassarre, *Phys. Rev. Lett.* **2023**, *130*, 256901.
[59] T. R. Ravindran, A. K. Arora, T. N. Sairam, *J. Raman Spectrosc.* **2007**, *38*, 283.
[60] E.-R. E. Mojica, N. Abbas, L. O. Wyan, J. Vedad, R. Z. B. Desamero, **2018**, in *ACS Symposium Series* (Ed.: M. D. Sonntag), American Chemical Society, Washington, DC, pp. 181–197.
[61] B. Wicher, R. Chodun, M. Trzcinski, K. Nowakowska - Langier, Ł. Skowroński, A. Lachowski, K. Zdunek, *Appl. Surf. Sci.* **2021**, *565*, 150540.
[62] Y. C. Choi, K.-I. Min, M. S. Jeong, *J. Nanomater.* **2013**, *2013*, 615915.

[63] C. Santoro, R. Gokhale, B. Mecheri, A. D'Epifanio, S. Licoccia, A. Serov, K. Artyushkova, P. Atanassov, *ChemSusChem* **2017**, *10*, 3243.
[64] A. G. Sault, *Appl. Surf. Sci.* **1994**, *74*, 249.
[65] M. Descostes, F. Mercier, N. Thromat, C. Beaucaire, M. Gautier-Soyer, *Appl. Surf. Sci.* **2000**, *165*, 288.
[66] C. M. Woodbridge, D. L. Pugmire, R. C. Johnson, N. M. Boag, M. A. Langell, *J. Phys. Chem. B* **2000**, *104*, 3085.
[67] M. Umaña, D. R. Rolison, R. Nowak, P. Daum, R. W. Murray, *Surf. Sci.* **1980**, *101*, 295.
[68] A. Nazir, H. Yu, L. Wang, Y. He, Q. Chen, B. U. Amin, D. Shen, *Appl. Phys. A* **2020**, *126*, 749.
[69] A. L. Goff, F. Moggia, N. Debou, P. Jegou, V. Artero, M. Fontecave, B. Jousselme, S. Palacin, *J. Electroanal. Chem.* **2010**, *641*, 57.
[70] M. Mullet, V. Khare, C. Ruby, *Surf. Interface Anal.* **2008**, *40*, 323.
[71] A. P. Grosvenor, B. A. Kobe, M. C. Biesinger, N. S. McIntyre, *Surf. Interface Anal.* **2004**, *36*, 1564.
[72] T.-C. Lin, G. Seshadri, J. A. Kelber, *Appl. Surf. Sci.* **1997**, *119*, 83.
[73] N. Chubar, V. Gerda, M. Szlachta, G. Yablokova, *Solid State Sci.* **2021**, *121*, 106752.
[74] H. Yano, E. Higuchi, H. Uchida, M. Watanabe, *J. Phys. Chem. B* **2006**, *110*, 16544.
[75] Y. Li, K. Xu, Q. Zhang, Z. Zheng, S. Li, Q. Zhao, C. Li, C. Dong, Z. Mei, F. Pan, S. Dou, *J. Energy Chem.* **2022**, *66*, 100.
[76] Y. Chen, X. Kong, Y. Wang, H. Ye, J. Gao, Y. Qiu, S. Wang, W. Zhao, Y. Wang, J. Zhou, Q. Yuan, *Chem. Eng. J.* **2023**, *454*, 140512.
[77] K. Li, J. Li, H. Yu, F. Lin, G. Feng, M. Jiang, D. Yuan, B. Yan, G. Chen, *Sci. Total Environ.* **2022**, *819*, 153115.
[78] S. Sun, F. Yang, X. Zhang, J. Qian, K. Wei, J. An, Y. Sun, S. Wang, X. Li, Y. Li, *Chem. Eng. J.* **2024**, *487*, 150673.
[79] T. Mineva, I. Matanovic, P. Atanassov, M.-T. Sougrati, L. Stievano, M. Clémancey, A. Kochem, J.-M. Latour, F. Jaouen, *ACS Catal.* **2019**, *9*, 9359.
[80] J. Li, M. T. Sougrati, A. Zitolo, J. M. Ablett, I. C. Oğuz, T. Mineva, I. Matanovic, P. Atanassov, Y. Huang, I. Zenyuk, A. Di Cicco, K. Kumar, L. Dubau, F. Maillard, G. Dražić, F. Jaouen, *Nat. Catal.* **2021**, *4*, 10.
[81] E. Schifano, G. Cavoto, F. Pandolfi, G. Pettinari, A. Apponi, A. Ruocco, D. Uccelletti, I. Rago, *Nanomaterials* **2023**, *13*, 1081.
[82] F. Sarasini, J. Tirillò, M. Lilli, M. P. Bracciale, P. E. Vullum, F. Berto, G. De Bellis, A. Tamburrano, G. Cavoto, F. Pandolfi, I. Rago, *Compos. Part B Eng.* **2022**, *243*, 110136.
[83] I. Rago, R. Rauti, M. Bevilacqua, I. Calaresu, A. Pozzato, M. Cibinel, M. Dalmiglio, C. Tavagnacco, A. Goldoni, D. Scaini, *Adv. Biosyst.* **2019**, *3*, 1800286.
[84] R. P. Yadav, I. Rago, F. Pandolfi, C. Mariani, A. Ruocco, S. Tayyab, A. Apponi, G. Cavoto, *Nucl. Instrum. Methods Phys. Res. Sect. Accel. Spectrometers Detect. Assoc. Equip.* **2024**, *1060*, 169081.
[85] V. Carpenella, F. Ripanti, E. Stellino, C. Fasolato, A. Nucara, C. Petrillo, L. Malavasi, P. Postorino, *J. Phys. Chem. C* **2023**, *127*, 2440.